PPH dendrimers grafted on silica nanoparticles: surface chemistry, characterization, silver colloids hosting and antibacterial activity†

Aurélien Hameau,[ab] Vincent Collière,[ab] Julien Grimoud,[c] Pierre Fau,[ab] Christine Roques,[c] Anne-Marie Caminade[ab] and Cédric-Olivier Turrin*[ab]

DOI: 10.1039/c3ra43348j

Polyphosphorhydrazone (PPH) dendrimers have been grafted on silica nanoparticles, and the surface functions of the dendrimers have been derivatized to phosphonates with lateral poly(ethyleneglycol) (PEG) chains. All materials have been thoroughly characterized by MAS NMR, FT-IR, electron microscopy, TGA and elemental analysis. These materials successfully hosted silver and silver oxide nanoparticles. The resulting composites exhibit antibacterial activity.

Introduction

The manipulation and the accurate functionalization of nano-objects is undoubtedly a promising and challenging field of research. In this regard, the association of soft and hard nano-objects, like dendrimers[1] and metal or metal oxide nanoparticles[2] (NPs) is offering unprecedented possibilities to reach high degrees of multifunctionalization, allowing to envision a large scope of applications. In this wide field of research, many efforts have been devoted to the production of dendrimer encapsulated metal NPs[3] or dendrimer-stabilized metal NPs.[4] Another active field of investigation encompasses dendrimer–silica hybrid mesoporous materials obtained by sol–gel procedures.[5,6] The interaction of small-sized, discrete silica particles, with dendrimers is more scarcely reported, and most of the work is dedicated to surface modification of silica NPs through a stepwise growth of dendrimer-like structures from reactive or initiator centres. For example, Tsubokawa *et al.* reported in a seminal work the stepwise outgrowth of hyperbranched polyamidoamine (PAMAM)-like structures on the surface of silica nanoparticles[7] having a mean diameter of 16 nm on which the amine initiator group was introduced by means of aminopropyltriethoxysilane (APTES). This strategy opened new perspectives for the design of dendrimer-modified silica-based stationary phases for chromatography purposes[8] or for the development of easily recyclable catalytic systems. In the latter case, the catalytic properties can be brought by metal complexes on the surface of the dendrimers,[9,10] or by transition metal NPs embedded in the dendrimeric architectures.[11] Alternatively, dendrimers can be covalently grafted on the surface of silica NPs by a direct post-synthesis silica modification through reactive or hooking centres. This strategy allows a higher control on the structural definition of the organic content of the final hybrid material, but invariably leads to a certain degree of reticulation of the inorganic building blocks due to dendrimer multivalency, even though it can be prevented by the use of dendrons instead of dendrimers. It should be noted that despite its attractiveness, this strategy is much less documented than the stepwise approach evoked above. In this respect, large silica NPs derived from MCM-41 mesoporous silica with a mean diameter of 250 nm have been loaded with a fluorescent dye, covalently modified with generation 2 PAMAM dendrimers through isocyanate hooking centres and then successfully assayed as transfection reagents.[12] Another example also involves large silica microspheres (100–400 nm) which have been covalently modified with generation 4 PAMAM dendrimers. For this purpose, epoxide hooking centres were generated on the silica microspheres in a two-step procedure by means of vinyltriethoxysilane. The silica-hooked dendrimers were further loaded with Pd(II) ion complexes. The reduction of the hybrid systems led to silica–dendrimer core–shell structures with dendrimer encapsulated NPs which were efficiently assayed and recycled in catalytic hydrogenation reactions.[13] In this example, the dendrimer scaffold affords a suitable environment for Pd NPs hosting. The hosting of metallic NPs on the surface or within silica networks can be

[a]*Laboratoire de Chimie de Coordination du CNRS, BP 44099, 205 route de Narbonne, 31077 Toulouse cedex 4, France. E-mail: turrin@lcc-toulouse.fr; Fax: 33 5615 5003*

[b]*Université de Toulouse, UPS, INPT, F-31077 Toulouse Cedex 4, France*

[c]*Laboratoire de Génie Chimique, UMR 5503, UPS, Faculté de Pharmacie, 35 chemin des Maraîchers, 31062 Toulouse cedex 9*

† Electronic supplementary information (ESI) available: Multinucleus MAS NMR spectra (CP-MAS and HPDEC experiments), FT-IR spectra, TGA and electronic microscopy and EDX data of the silica **Si-1** to **Si-5**, NMR data and mass spectrometry data of compound **2a** to **2d**, FT-IR and CP-MAS NMR data of starting dendrimer **1**, pictures of MBC cultures and data related to the adsorption test experiment. See DOI: 10.1039/c3ra43348j

achieved according to a large variety of processes. In the case of silver NPs containing silica, catalytic,[14] antibacterial[15] or sensing properties can be obtained.[16] Nevertheless, most of these synthetic techniques are not compatible with the incorporation of organic materials which can offer complementary functionalities to the final material, in addition to the NP-stabilizing ones. It is the case of one-pot sol–gel processes which require silica-densifying steps under harsh conditions[17] or co-precipitation under strong acidic conditions.[15] Alternative strategies involve surface decoration of preformed silica networks with stabilizing functions.[15] To the best of our knowledge, hyperbranched macromolecules, which have proved to offer excellent silver NPs stabilising properties in homogeneous conditions,[18] have not been used to achieve such purposes on silica surfaces.

Phosphorus-containing dendrimers, also coined as poly (phosphorhydrazone) (PPH) dendrimers,[19] have also been used to prepare silica-based materials incorporating covalently bonded PPH architectures. We have described the synthesis of mesostructured silica bulk materials according to sol–gel procedures involving siloxane-cored PPH dendrons.[6] Alternatively, the covalent grafting of PPH dendrimers on silica can be envisaged through a multivalent attachment involving the surface groups of symmetrical dendrimers. In this regard, our group has developed a strong expertise on the covalent immobilization of PPH dendrimers onto glass slides.[20] This technique, which was made possible by preliminary experiments on quartz surfaces modified with APTES,[21] has led to the development of sensors, namely dendrichips™. Nevertheless, we have never explored in-depth structural and spectroscopic investigations on the nature of the hybrid interface related to the use of bulk support (glass, mica, quartz plates).

Herein we describe a stepwise process to modify the surface of finely divided silica NPs with a simple surface derivatization approach using PPH dendrimers which offers post-synthesis possibilities for surface modification of the final hybrid nanocomposites. The work described in this report is based on a straightforward transfer of the APTES-mediated grafting strategy to finely divided material, namely silica NPs, which allows better spectroscopic description of the hybrid interface thanks to FT-IR and MAS-NMR analyses. Additionally, the functional versatility of our *nano onto nano* approach, offered by the highly reactive PPH surface, is illustrated with the preparation of PEG–aminophosphonate surface functions which have never been described on dendrimeric architectures. The applicability of these new highly functional nanocomposites is illustrated by the efficient hosting of tiny silvers NPs and the preliminary evaluation of the bacteriostatic and bactericidal properties of these materials.

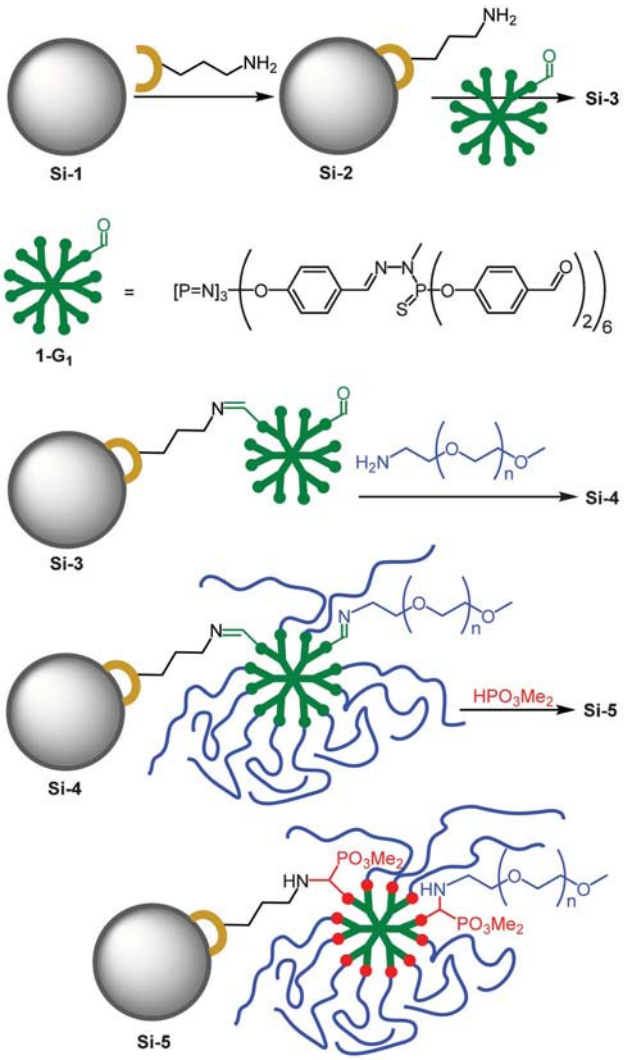

Fig. 1 Schematic representation of the strategy for dendrimer grafting and post-synthesis functionalization. The drawing is not scaled for clarity purposes, NPs are in reality *ca.* 5 times bigger than dendrimers and can be attached by several dendrimers.

Results and discussion

Chemistry

We have chosen to work on a simple water-releasing condensation reaction between aldehyde terminated PPH dendrimers and amine-bearing NPs. This reaction allows the creation of a reliable covalent bonding of the PPH dendrimers onto the surface of the nanoparticles according to routine-like procedures, in the view of creating chemical modifications which can be easily monitored by readily accessible spectroscopic methods. This grafting strategy (Fig. 1), as mentioned above, has been successfully developed to immobilize high generation PPH onto macroscopic glass substrates[21] for the large-scale production of dendrislides™ and dendrichips™.[20] The grafted dendrimer layer can further undergo chemical transformations and the overall process can be easily monitored by MAS NMR and FTIR techniques to follow the chemical modifications that are made on the nanocomposites. Commercially available silica nanoparticles (mean diameter 12 nm) were activated by thermal treatment (**Si-1**), and the creation of active Si–OH moieties was unambiguously detected on FTIR spectra by a sharp band centred on 3747 cm^{-1} (see

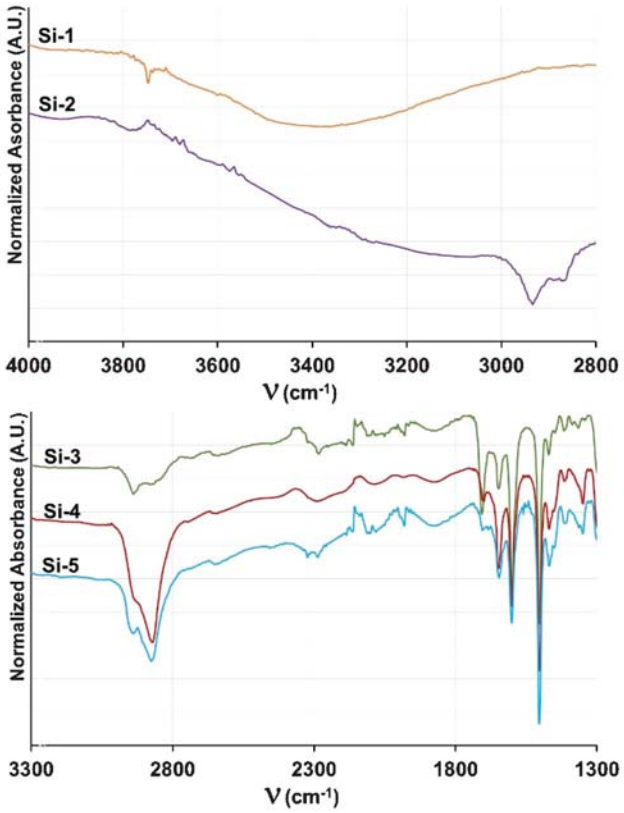

Fig. 2 FT-IR monitoring of the synthesis of modified silica. Spectra are normalized and data have been offset for clarity (reference at 1046 cm^{-1} for **Si-1** and **Si-2** and 1500 cm^{-1} for **Si-3**, **Si-4** and **Si-5**).

Fig. 2 and ESI†). Activated **Si-1** was then derivatized with (3-aminopropyl)triethoxysilane (APTES) according to standard procedures.[22] The resulting amino-silanized silica NPs **Si-2** were treated with a large excess of first generation aldehyde-terminated PPH dendrimer[19] **1-G$_1$** in a THF–methanol mixture at 55 °C.

Having in hands these dendrimer-capped silica NPs **Si-3**, the unreacted aldehyde functions were further condensed with an amine-functionalized poly(ethyleneglycol) (PEG) **2d** (Scheme 1) having an average weight of 560 g mol^{-1}, containing roughly 11 ethylene glycol moieties. The latter was prepared from commercial methoxy–PEG (MW ~ 550 g mol^{-1}) **2a** on a 10 g scale according to a routine procedure[23] involving the corresponding Mesyl-PEG **2b** and azido-PEG **2c** as intermediates (Scheme 1). This intermediate was reduced in a one-pot, two-step procedure involving a Staudinger reaction with

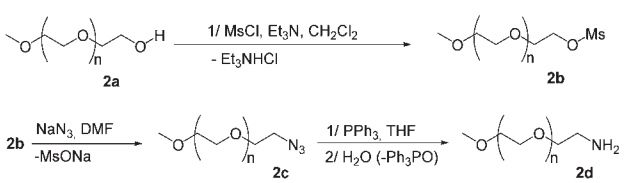

Scheme 1 Synthesis of PEG derivative **2d**.

triphenylphosphine and subsequent hydrolysis of the resulting iminophosphorane. This sequence was preferred to the alternative catalytic hydrogenolysis of the azide which is always accompanied by entrapment of transition metal residues in the PEG moieties, easily detectable by the darkening of the PEG compound. The weight distribution of the resulting amino-PEG **2d** was found to be similar to the one of the starting commercial PEG **2a**, as determined by mass spectrometry (see ESI†). The length of the PEG was elicited in order to provide efficient PEG capping to the dendrimer-modified NPs without preventing complete condensation of the aldehyde functions, which might be most difficult to achieve with long-chained PEGs.

During the grafting of dendrimer **Si-3** onto the surface of **Si-2**, the information provided by FTIR and ^{13}C CP-MAS NMR (see next sections) showed a significant decrease of the intensity of the aldehyde signals. It was then assumed that the covalent immobilization of dendrimer **1-G$_1$** involved several of the twelve aldehyde functions of each dendrimer. To evaluate the number of remaining reactive aldehyde functions, we have reacted a small amount of **Si-3** with incremented quantities of amino-PEG **2d** (0.5 eq. per increment). The consumption of the amine was followed on TLC plates. After addition of 5 equivalents of amino-PEG **2d** per grafted dendrimer, traces of unreacted **2d** were detected in the supernatant. This procedure allowed us to assume that dendrimers immobilized on **Si-3** are connected to the silica surface through *ca.* 7 imine bonds.

The small quantity of unreacted PEG was not removed after the imination step to prevent the risk of hydrolysis of the imine, and also to favour the completion of the next step reaction. The hydrophosphorylation of Schiff bases with dialkyl phosphite, which can be considered as a Pudovik reaction applied to azomethines, or a Kabachnik-Fields reaction, can be performed in two separate steps with isolation of the intermediate imine, or in one pot,[24] all components being added at once, and in both cases the mechanism of this reaction remains unclear.[25,26] This hydrophosphorylation step was run in the presence of an excess of dimethyl phosphite used as solvent, as previously described for other PPH dendrimers in homogeneous conditions.[27] All materials were fully characterized by FTIR and ^{13}C, ^{31}P and ^{29}Si MAS NMR spectroscopies, which gave complementary information. Proton MAS NMR spectroscopy resulted in very broad signals (see ESI†). The organic loading was studied by TGA and confirmed by elemental analysis. Transmission Electronic Microscopy was also used to image the modified silica NPs.

FTIR analysis

After the first chemical modification of the silica NPs, the signature of the alkylamine on normalized FTIR spectrum was found to be rather weak on **Si-2** (Fig. 2). Actually, only a weak C–H asymmetrical stretching band at 2933 cm^{-1} and a weak C–H bending band at 1472 cm^{-1} were detectable, along with a strong Si–O stretching band at 1055 cm^{-1} and a Si–O bending band at 800 cm^{-1} (not shown).

The presence of imine bonds on the surface of **Si-3** was evidenced by a typical stretching band at 1645 cm^{-1} (Fig. 2) located between the aldehyde stretching band at 1705 cm^{-1}

and an aromatic stretching band at 1600 cm^{-1}, this imine band being not observed on the starting material **1-G$_1$** (see ESI†). It should be noted that no trace of adsorbed dendrimer **1-G$_1$** was detected by NMR or IR spectroscopies, proving the efficiency of the washing sequence with a THF/dichloromethane mixture on sintered glass filter plate. This finding was confirmed by an adsorption test reaction run under routine conditions. Typically the reaction between dendrimer **1-G$_1$** (100 mg) and the activated, but not functionalized silica **Si-1** (150 mg) in a methanol/THF (5 : 2, *v*/*v*) at 55 °C overnight showed that no trace of adsorbed dendrimer was detected after the washing sequence (see ESI†). Following this step, the unreacted aldehyde functions were reacted with PEG derivative **2d** to afford **Si-4**. The aldehyde stretching band (1705 cm^{-1}) dramatically vanishes during this step while the imine stretching band at 1645 cm^{-1} increases. Nevertheless a very weak aldehyde stretching band was found to remain, traducing the presence of traces of unreacted aldehydes, contrarily to what is observed when the reaction is performed with the free dendrimer **1-G$_1$** in homogeneous conditions.[28] This condensation reaction was assumed to be almost complete on the basis of FTIR and CP-MAS NMR analysis (see next section), and the traces of unreacted aldehyde could not be determined.

The following hydrophosphorylation of **Si-4** was also monitored by FTIR analysis (Fig. 2), but this technique did not allow to ascertain the complete transformation of the imine functions as the stretching band of the imine at 1648 cm^{-1} overlays with the bending band of the secondary amine which is generated during the reaction. The signature of residual aldehyde function is still noticeable with presence of a very weak band at 1700 cm^{-1}, confirming the existence of a few unreactive sites. Nevertheless it must be noted that during this step the intensity of the residual aldehyde fades. This observation can be related to a possible condensation completion thanks to the presence of remaining PEG derivative **2d** which was not removed at the previous step.

NMR analysis

MAS NMR analysis proved to be a valuable tool for structural analysis of the modified silica NPs. On **Si-2** material, the presence of signals at −59 and −67 ppm on ^{29}Si CP-MAS NMR spectra, corresponding to T_2 and T_3 silicon atoms respectively, confirmed the presence of covalently bonded aminopropyl residues.[29] Comparison of the ^{29}Si CP-MAS NMR spectra of the grafted silica NPs showed that the inorganic component of the hybrid systems is not affected by the complete reaction sequence (Fig. 3).

Accurate information was provided by ^{13}C CP-MAS NMR analysis. On the spectrum of **Si-2** three signals at 9.7, 26.9 and 43.3 ppm were detected, corresponding to the methylene groups of the aminopropyl linker (Fig. 4). The next chemical modification involving the covalent grafting of dendrimer **1-G$_1$** on the amine-bearing silica NPs **Si-2** was easily monitored by this technique. The rise of a signal at 160 ppm attributed to the CH=N linkage was observed along with a fair decrease in the intensity of the signal at 190 ppm attributed to the unreacted aldehydes. Other typical signals of the grafted dendrimer **1-G$_1$** were not significantly affected by the

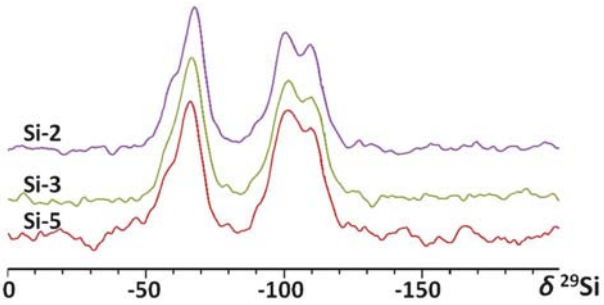

Fig. 3 ^{29}Si CP-MAS NMR monitoring of the synthesis of modified silica.

immobilization. Signals corresponding to the unreacted aminopropyl linker were still remarkably detectable on **Si-3**, indicating incomplete reaction of the amine groups, as expected if one considers the presence of strongly interacting amine groups with the silica surface[30] (Fig. 4). In detail, a signal at 43 ppm confirmed the presence of unreacted –CH_2–NH_2, this signal being already present on the ^{13}C–{^{1}H} CP-MAS NMR spectrum of **Si-2**. After condensation, a new signal at 62.6 ppm rises, and can unambiguously be attributed to the same methylene group neighbouring the imine formed during this grafting step (CH_2–N=CH). As detailed in the chemistry section, it was deduced that dendrimers immobilized on **Si-3** are connected to the silica surface through *ca.* 7 imine bonds (Fig. 4). This can be related to the significant decrease of the aldehyde signal on ^{13}C–{^{1}H} CP-MAS NMR and FTIR spectra (see previous section). This multiple attachment is allowed by the flexibility of the PPH dendrimer scaffold, as previously observed with high generation dendrimers which can flatten onto silica surfaces.[31]

The ^{13}C{^{1}H} CP-MAS NMR spectrum of material **Si-4** also confirmed the condensation of aldehyde function by almost complete disappearance of the CHO signal at 189.9 ppm, and the signal at 161.1 ppm was unambiguously attributed to the imine bond formed during this step (Fig. 5). The fact that residual aldehyde functions were still detectable after longer times of reaction (up to 2 days) and despite the use of non-sterically impaired, short-chained PEG **2d**, was attributed to

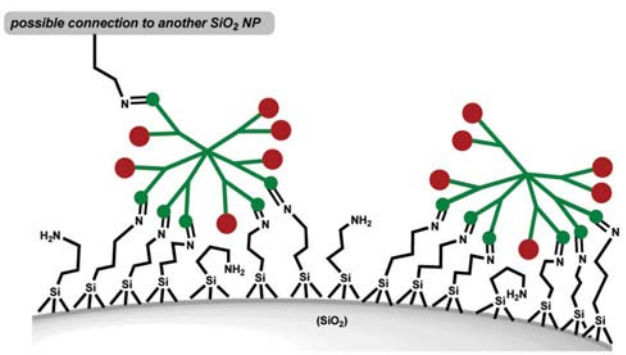

Fig. 4 Schematic representation of the surface of **Si-2** with unreacted aldehyde functions (red dots).

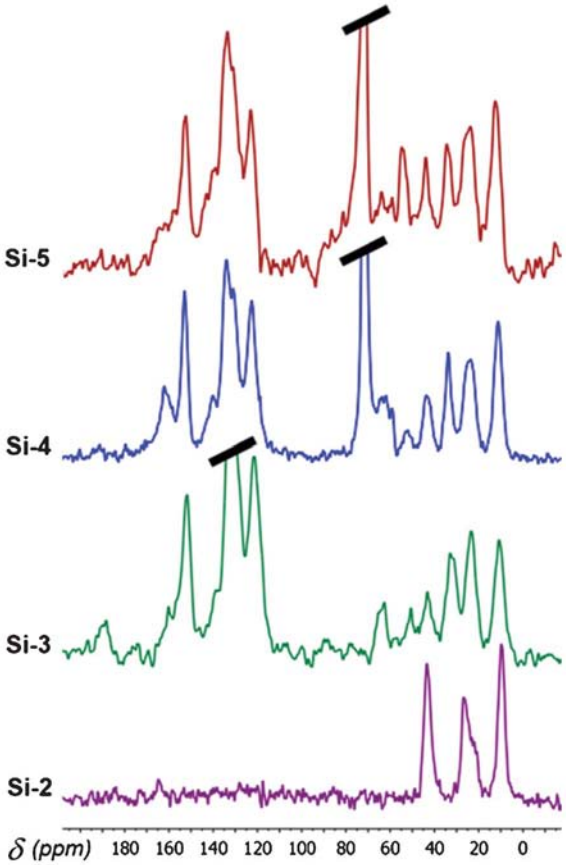

Fig. 5 ^{13}C CP-MAS NMR monitoring of the synthesis of modified silica.

the presence of unreactive and confined aldehyde function most possibly facing the silica surface.

In the case of **Si-5**, the complete disappearance of the imine group at 160 ppm is observed, while typical signals of the amino-methylenephosphonate are detected at 53 and 61 ppm for the P–OMe and the CH–P groups respectively. As discussed above, the FTIR analysis of materials **Si-4** and **Si-5** revealed the presence of traces of aldehyde functions which were not transformed into imines even in the presence of an excess of amino-PEG **2d**. The aldehyde signature at *ca.* 190 ppm is not easy to detect on 13C CP-MAS NMR spectra of **Si-4** and **Si-5**. This is due to the fact that amorphous samples usually give broadened CP-MAS NMR signals, and in our case the observation of such small proportions of unreacted aldehyde functions is less obvious.

Complementary information was provided by $^{31}P\{^{1}H\}$ CP-MAS NMR analysis of **Si-5**, which shows the presence of a typical signal at 25.8 ppm for the aminophosphonate moieties (Fig. 6). Other signals at *ca.* 60 and 8 ppm are also observable on the $^{31}P\{^{1}H\}$ CP-MAS NMR spectra of **Si-3** and **Si-4**, and are attributed to the internal thiophosphorus and cyclotriphosphazene moieties respectively.

Thermogravimetric and elemental analysis

The weak spectroscopic signature of the aminopropyl groups grafted on **Si-2** can be correlated to a low organic content of

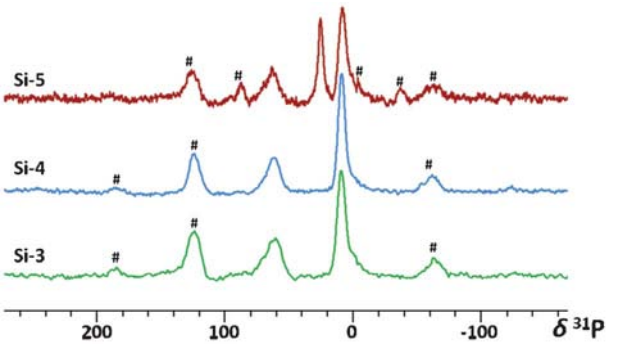

Fig. 6 ^{31}P CP-MAS NMR monitoring of the synthesis of modified silica (# indicate rotation bands).

the amino-silanized silica NPs. **Si-2** silica NPs exhibit a 6.7% weight loss between 200 °C and 1000 °C by thermogravimetric analysis (TGA, Fig. 7 and ESI†). This value roughly corresponds to a 1.15 mmol g^{-1} content in reactive amines.

The organic weight fraction of **Si-2** deduced from TGA corresponds to a 6.5% weight fraction and a 6.7% organic molar fraction, hence the formula of **Si-2** would be $(SiO_2)_{93.3}(C_3H_8N)_{6.7}$. For **Si-3**, the incremented organic content can also be rapidly deduced from TGA analysis. The TGA weight loss of **Si-3** over the same temperature range is 15.5%. The relative contribution of the aminopropyl residue deduced above being constant, the residual incremented contribution for dendrimer **1-G$_1$** is 9%. Taking into account that dendrimer **1-G$_1$** loses only 51.2% of its weight under the same thermal conditions (between 200 °C and 1000 °C under nitrogen), the relative weight fraction of **1-G$_1$** to **Si-3** is 17.6%, leading to the following weight fractions: $[(SiO_2)_{93.5}(C_3H_8N)_{6.5}]_{82.4}$(**1-G$_1$**)$_{17.6}$, or $(SiO_2)_{77.04}(C_3H_8N)_{5.36}$(**1-G$_1$**)$_{17.6}$. From this expression, the crude formula of **Si-3** can be expressed as $(SiO_2)_{92.87}(C_3H_8N)_{6.68}$(**1-G$_1$**)$_{0.45}$. This formula indicates that the aminopropyl anchor/dendrimer ratio is close to 15. Taking into account that 7 aldehyde functions of **1-G$_1$** are involved (out of twelve) in the covalent immobilization on silica, this finding indicates that *ca.* half of the aminopropyl

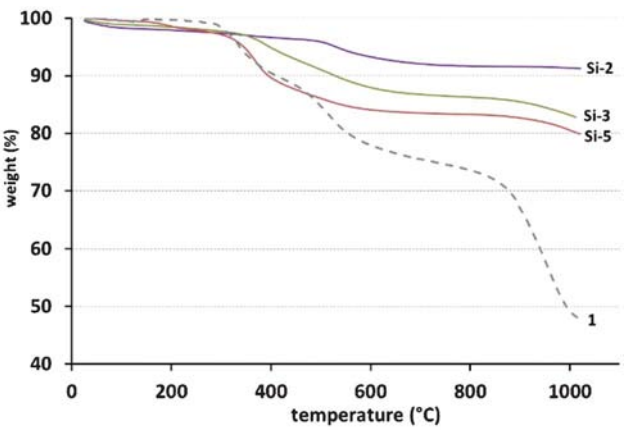

Fig. 7 Thermogravimetric analysis (TGA) under nitrogen.

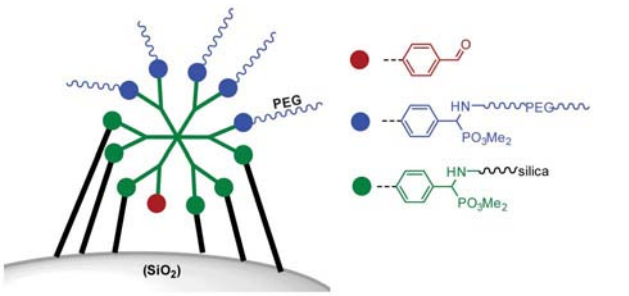

Fig. 8 Possible connecting distribution of dendrimers grafted on the surface of **Si-5**.

groups are not involved in the dendrimer immobilization step. This point is in agreement with ^{13}C CP-MAS NMR analysis which show that a significant amount of aminopropyl groups is not affected by the immobilization step.

The obtaining of an approximate formula for **Si-5** is much less direct. Considering the FTIR and CP-MAS NMR results (almost complete disappearance of the aldehyde signals), it can be assumed that almost all the aldehyde functions are transformed to aminophosphonates. If one considers that 5 aldehyde functions per dendrimer are condensed with amino-PEG **2d**, and assuming a complete phosphorylation reaction, each dendrimer grafted on **Si-5** would bear, in average, 5 amino-PEG-phosphonate groups, roughly 6 silica-connecting amino-phosphonate groups, and 1 unreacted aldehyde group (Fig. 8).

From these hypotheses supported by experimental data, the weight fraction of amino-PEG **2d** ($C_{25}H_{51}NO_{12}$, MW ~ 558 g mol^{-1}) in **Si-5** would be 13%, and then the weight fraction of each incremented component would lead to the following expression: $[(SiO_2)_{77.04\%}(C_3H_8N)_{5.36\%}(\mathbf{1'\text{-}G_1})_{17.6\%}]_{87}(\mathbf{2d})_{13}$, where $\mathbf{1'\text{-}G_1}$ stands for a theoretical dendrimer having 9 aminophosphonate groups (without the weight contribution of both the aminopropyl groups and the amino-PEG component) and 3 residual insaturations CH=N and CHO ($C_{150}H_{173}N_{15}O_{47}P_{18}S_6$ MW ~ 3688 g mol^{-1}). From this expression, the crude formula of **Si-5** can be expressed as $(SiO_2)_{91.183}(C_3H_8N)_{6.573}(C_{150}H_{173}N_{15}O_{54}P_{21}S_6)_{0.339}(C_{25}H_{51}NO_{12})_{1.905}$. It must be noted that the **Si-5** weight loss measured by TGA cannot be directly correlated to its composition or organic content, mostly because it is impossible to predict the weight loss of a theoretical dendrimer having on the surface the connecting distribution deduced above (Fig. 8), the thermal degradation of PPH dendrimer being highly dependent on the nature of their surface functions.[32] The data obtained from TGA have been compared to elemental analysis obtained for **Si-2**, **Si-3** and **Si-5** (Table 1). For all materials, the Si/C and Si/P or (Si/N) ratios have been compared, and in most cases the deviation is lower than 10%, except for **Si-2** which exhibits a higher carbon content than the predicted content obtained from TGA analysis. Taking into account the necessary approximations that have been made to operate the TGA data, the fact that both techniques give comparable results significantly confirms the possible surface functions distribution of the final material **Si-5** and the fashion in which these organic functions are incremented on the surface of silica NPs.

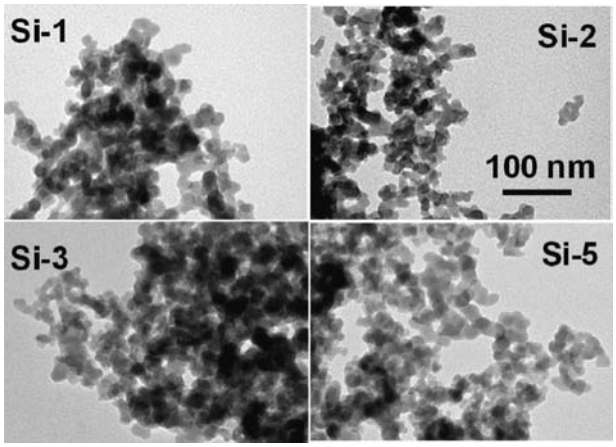

Fig. 9 TEM imaging of isolated silica **Si-1**, **Si-2**, **Si-3** and **Si-5**.

Imaging techniques

TEM imaging of the NPs showed the absence of significant geometrical modification (Fig. 9), confirming the observations of ^{29}Si CP-MAS NMR monitoring. Typically, the starting naked silica NPs were found to be already significantly aggregated, and aggregation was observed for **Si-1**, **Si-2** and **Si-3**. One could expect reduction of the aggregation thanks to the organic coating,[33] but during the preparation of **Si-3**, the aggregation *via* dendrimer mediated reticulation cannot be excluded, despite careful dilution of the silica nanoparticles and relatively smooth reaction conditions. Finally, the presence of isolated NPs was scarcely detected in all cases, and the mean diameter of NPs was found to be rather constant and close to the data provided by the commercial source of the naked native silica, that is roughly 10 to 15 nm.

Energy-dispersive X-ray (EDX) spectroscopy confirmed the presence of organic materials on the silica NPs (see ESI†). The typical signature of the PPH dendrimer can be detected on **Si-3**

Table 1 TGA and elemental analysis

Si-X	Chemical composition from TGA analysis	Si/C ratio		Si/P or Si/N ratio	
		from TGA	from elemental analysis	from TGA	from elemental analysis
Si-2	$(SiO_2)_{93.3}(C_3H_8N)_{6.7}$	4.65	3.45	13.92 (Si/N)	13.37 (Si/N)
Si-3	$(SiO_2)_{92.87}(C_3H_8N)_{6.68}(\mathbf{1\text{-}G_1})_{0.45}$	1.16	1.01	22.97 (Si/P)	22.12 (Si/P)
Si-5	$(SiO_2)_{91.183}(C_3H_8N)_{6.573}(C_{150}H_{173}N_{15}O_{54}P_{21}S_6)_{0.339}(C_{25}H_{51}NO_{12})_{1.905}$	0.77	0.74	15.01 (Si/P)	14.71 (Si/P)

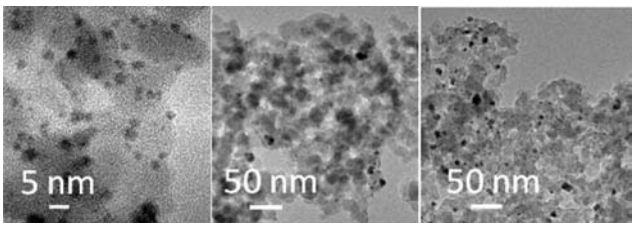

Fig. 10 HRTEM imaging of silver species condensed on **Si-2** (left), **Si-3** (middle) and **Si-5** (right), which appear as black dots in the silica matrix (grey).

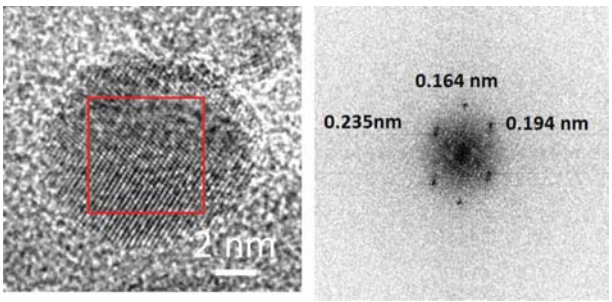

Fig. 11 HRTEM image of a single Ag oxide nanoparticle on sample **Si-2** (left) and the corresponding Fourier transformation attributed to Ag_2O structure (right) (the red square corresponds to the analysis zone).

and **Si-5** materials at 2.01 eV (phosphorus), whereas the presence of aminopropyl group is hardly detectable on **Si-2** with a weak signal at 0.39 eV (nitrogen) shouldering the oxygen absorption signal located at 0.523 eV.

Ag NPs hosted on dendrimer-modified SiO_2 NPs

Addition of silver acetate in a water suspension of modified silica **Si-X** (X = 2, 3 or 5) with a typical metal/silica ratio close to 1 : 10 (*w*/*w*) led to the darkening of silica suspensions, whereas the liquid phase, upon decantation, remained colorless. This color change, traducing the formation of silver colloids, was observable after a few minutes and increased with time. TEM and HRTEM imaging of the suspensions confirmed the presence of silver colloids on the grafted silicas, whereas no nano-object could be found away from silica. Same observations were made in the absence of light. When the colloidal growth is run in the absence of reducing agent, it appears that the degree of functionalization of the hosting silica clearly influences the size and size distribution of condensed silver colloids onto the silica (Fig. 10). Actually, the Ag particles are rather homogeneously condensed on silica with grafted amines (**Si-2**), and display a very low mean size with a narrow size distribution (Table 2). When more bulky molecules bearing new chemical functions (**Si-3** and **Si-5**) are grafted on the silica, the deposition mechanism generally evolves towards the deposition of larger silver particles, with broader size distributions (Fig. 10 and Table 2).

EDX analysis also confirmed that the silver NPs were present only in the vicinity of modified silica, X-ray emissions of phosphorus, silicon and silver atoms being systematically co-located (see ESI†). UV-vis analysis of both the transparent liquid phases (after decantation) and the suspensions revealed the absence of plasmonic absorption in all cases (Fig. 12), even after 2 weeks, excluding the formation of metallic silver colloids under these conditions. In addition, as revealed by HRTEM analysis, the crystallinity of the condensed silver species is low at that stage. Nevertheless, on selected areas of the particles we applied a Fourier transformation in order to evidence the corresponding crystal patterns (Fig. 11). The results indicated the presence of various silver oxide structures (AgO, Ag_2O, Ag_3O...) on the different analyzed NPs, although in some cases the presence of metallic silver cannot be fully ruled out (Table 2, ESI†). The absence of UV-Vis absorption in such cases must be related either in the very low quantity of metallic silver compared to the oxide phase, and/or to very small metallic cluster displaying no plasmon resonance due to size effects.

The growth of silver NPs with these modified silica was then repeated with the same metal/silica ratio (1 : 10, *w*/*w*) in the presence of sodium borohydride as a reducing agent which was added after one hour of stirring (Table 2, entries 4–6). Under these conditions, the darkening of the silica suspen-

Table 2 Silver NPs data

Entry	Compound	Size distribution[a] min-max[a]	λ plasmon band (nm)	Crystalline network[b]
1	**Ag^{II}@Si-2**	1.9 (0.9) 1–7	—[c]	silver oxide[d]
2	**Ag^{II}@Si-3**	6 (6.8) 1–40	—[c]	silver oxide
3	**Ag^{II}@Si-5**	4.1 (3.5) 1–18	—[c]	silver oxide[d]
4	**Ag^{0}@Si-2**	8.5 (5.6) 3–30	416	silver
5	**Ag^{0}@Si-3**	5.5 (5.0) 1–38	394	silver[e]
6	**Ag^{0}@Si-5**	13.4 (10.9) 3–60	412	silver

[a] Mean size and standard deviation calculated from TEM and HRTEM images are given in nanometers, minimum and maximum diameters are also indicated. [b] From HRTEM. [c] No plasmon absorption band observed. [d] The presence of metallic silver NPs cannot be ruled out. [e] The sample was also found to contain silver oxide.

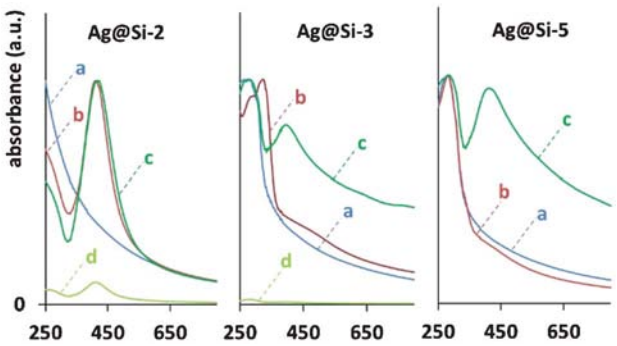

Fig. 12 UV-vis absorption spectra. a: **Ag^{II}@Si-X**, b: **Ag^{II}@Si-X** after reduction at day14, c: **Ag^{0}@Si-X**, d: **Ag^{0}@Si-X** after decantation. X = 2 (left), 3 (middle), 5 (right).

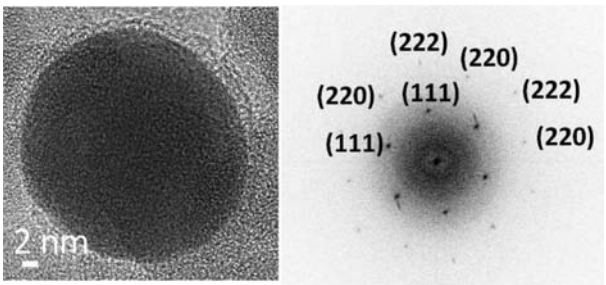

Fig. 13 HRTEM imaging of a Ag NP on **Si-5** (left) and Fourier transform diffraction pattern (right).

sions was also rapidly observed. The resulting **Ag^{0}@Si-X** (X = 2, 3, 5) were found to be located only on silica. Again, the influence of the grafted dendrimer on the silver NPs morphology was hard to rationalize as the colloids were found to have a rather large size distribution, between 2 and 30 nm for **Ag^{0}@Si-2** and **Ag^{0}@Si-3** and 2 to 70 nm for **Ag^{0}@Si-5** (Table 2). The mean size of the silver particles is higher after reduction in the case of **Si-2** and **Si-5**, indicating that after 1 h the condensation process is not achieved and once the reduction has started, more Ag species are still available for particle growth on the silica surface. Such phenomenon is not observed for **Si-3** since the mean size of the particles is similar before and after oxidation. This indicates that the silver species are poorly condensed on the moieties bearing the aldehydes functions compared to the two other cases (amines or PEG/phosphonate functions), a hypothesis which is supported by the good stabilizing properties of amines, phosphonates and PEGs, in comparison to those of aldehydes.

Contrarily to what was observed in the absence of reducing agent, the UV-vis analysis of an aliquot of the **Ag^{0}@Si-X** (X = 2, 3, 5) suspensions revealed a typical plasmon absorption band centred between 394 and 416 nm (Fig. 12), indicating the presence of metallic silver NPs. The absorption band for **Ag^{0}@Si-3** presents a much lower intensity correlated with a broad shape, in comparison with the absorption spectrum of **Ag^{0}@Si-2**. This observation is in accordance with the TEM characterization of this sample which displays both low particle mean size (5.5 nm) and the highest dispersion level. Additionally, one should notice the presence of a strong absorption band centred on 290–300 nm for **Si-3** and **Si-4** sample which can be unambiguously attributed to the dendrimer absorption.

Upon decantation, the UV spectra vanished almost to zero in all cases, confirming the fact that the silver NPs are located only onto the grafted silicas. The Fourier transform diffraction patterns obtained from HRTEM images confirmed the face-centered cubic structure of the Ag NPs obtained after reduction, as shown on a typical sample obtained with **Si-5** (Fig. 13).

Antibacterial activity

The antibacterial activity of the silver-loaded nanoparticles was estimated by determining the Minimal Inhibitory Concentration (MIC) and the Minimal Bactericidal Concentration (MCB) on 4 typical bacterial strains[34] (Table 3), two Gram-negative bacteria (*E. coli* CIP 103571 and *P. aeruginosa* CIP 1041161), and two Gram-positive bacteria (*S. aureus* CIP 4.83 and *E. hirae* CIP 58.55).[35] All samples were carefully decanted and centrifuged prior to bactericidal evaluation. As expected in the absence of silver (entry 1), no antibacterial activity was observed. In all cases the silver-loaded silica NPs exhibited bacteriostatic activities against all bacterial strains in the 50–500 ppm range (silver equivalents).

Table 3 MIC and MBC determined on 4 typical bacterial strains

Entry	Compound	*S. aureus* CIP 4.83 (Gram +)		*E. hirae* CIP 58.55 (Gram +)		*E. coli* CIP 103571 (Gram −)		*P. aeruginosa* CIP 104116 (Gram −)	
		MIC[a]	MBC[a]	MIC[a]	MBC[a]	MIC[a]	MBC[a]	MIC[a]	MBC[a]
1	**Si-2, Si-3, Si-5**	—	—	—	—	—	—	—	—
2	**Ag^{0}@Si-2**	62.5–125	>500	125	>500	62.5	500–1000	62.5	>500
3	**Ag^{II}@Si-2**	125–250	250	125	>500	62.5	500–1000	62.5–125	250
4	**Ag^{0}@Si-3**	125–250	250–500	31.25–62.5	>250	62.5	>250	125	250–500
5	**Ag^{II}@Si-3**	62.5–125	250–500	62.5	>250	62.5	>250	31.25	250–500
6	**Ag^{0}@Si-5**	500	>500	250	>500	250	500–1000	250	>500
7	**Ag^{II}@Si-5**	50–62.5	>500	25–31.25	>500	50–62.5	250	25–31.25	250
8	**CH_3COOAg**	15.63	500	7.81	>500	7.81	15.63	3.91	15.63

[a] In ppm (silver equivalents). Experiments have been performed once or twice, each time in duplicates: when two values are given, the estimated minimum concentration lies in-between these values.

Bactericidal effects have also been observed in some cases, but one should note that all activities were found to be lower than the ones measured for silver acetate. This finding can be related to the fact that in the case of colloidal silver, only a tiny portion of the overall metal content is potentially interacting with the microorganisms.

Interestingly, a small difference was observed between Gram-positive and Gram-negative strains for all materials and for silver acetate. In this regard, Gram-positive bacteria were found to be slightly less susceptible than Gram-negative bacteria which is in agreement with previous reports.[36] The antimicrobial property of silver is due to the ability of its ionized form to cause damage to cells by interacting with thiol-containing proteins and DNA.[37] In this respect, the antibacterial activity of silver colloids is also related to their ability to release ionized silver. Nevertheless the antibacterial property of silver NPs is highly related to their size,[38] the smaller ones being more active.[39] This latter finding is related to the higher percentage of surface atoms, which are prone to release silver ions, in small NPs. Despite the fact that we have observed by TEM and HRTEM that all silica-grafted silver NPs have quite large size distribution, between 1 and 20 nm, the size could be more critical than oxidation state. In the case of **Si-3** system, Ag^0 and Ag^{II} NPs have roughly the same average size, and **Ag^{II}@Si-3** is slightly more active than **Ag^0@Si-3**. In this case the difference of activity can putatively be related to ion release ability. In the case of **Si-2** and **Si-5** systems, Ag^{II} colloids are much smaller than Ag^0 colloids and significantly exhibit better activity.

Conclusions

Our strategy leads to highly functional PEG-phosphonate-dendrimer coated silica NPs. The covalent hybrid interface has been fully described by means of routine spectroscopic techniques such as FT-IR and MAS NMR. This straightforward strategy is easily amenable to other functional surfaces and other dendrimeric species, and the versatility of dendrimer surface chemistry could open exciting perspectives for applications in the fields of nanomaterials, catalysis and drug-delivery. In order to illustrate these possibilities, silver nanoparticles have been grown on these dendrimer modified silicas in a very simple fashion, and the resulting materials were found to exhibit preserved antibacterial activities. We are currently investigating the versatility of this strategy with other supporting nanoparticles and other colloidal systems.

Experimental section

General procedures and instrumentation

All reactions were carried out in the absence of air using standard Schlenk techniques and vacuum-line manipulations when carried out in organic solvents. Commercial samples (Acros, Fluka, Aldrich) were used as received. Solvents were dried and distilled according to routine procedure before use. Commercial silica was activated by thermal treatment (250 °C for 24 h) to afford **Si-1**. ^{1}H, ^{13}C, ^{31}P NMR, HMQC and HMBC measurements were performed on Bruker AV 300, DPX 300, AV 400, Avance 400 WB (solid state) and Avance 500. Coupling constants are reported in Hz and chemical shifts in ppm/TMS for ^{1}H and ^{13}C. Chemical shifts for ^{31}P spectra are calibrated with phosphoric acid as an external reference. The first-order peak patterns are indicated as s (singlet), d (doublet), t (triplet), q (quadruplet), qn (quintuplet). Complex non-first-order signals are indicated as m (multiplet). ^{13}C NMR signals were assigned using HMQC and HMBC sequences when required. UV-Vis spectra were recorded on a Perkin Elmer Lambda 35. FTIR spectra were recorded on a Perkin Elmer GX 2000. Spectra were normalized on signals that are not affected by the chemical modifications: 1046 cm^{-1} for **Si-1** and **Si-2** and 1500 cm^{-1} for **Si-3**, **Si-4** and **Si-5**. Mass spectroscopy was performed on a Waters MALDI micro MX and Xevo Q Tof spectrometers. A small drop of colloidal solution was deposited on a grid to perform the TEM, HRTEM, STEM and EDX analyses. The grid was home-made from a commercial copper grid (diameter 3.05 mm) which was covered by a thin collodion membrane, on which carbon was evaporated (approximately 50 nm thickness). Low resolution TEM analyses were performed on a JEOL JEM 1011 (100 kV, resolution 4 Å). A wide angle Megaview III (SIS) camera was used for routine imaging. High resolution TEM analyses and EDX analyses were performed on the TEM-FEG (Field Emission Gun) JEOL JEM 2100F (200 kV, resolution 2.3 Å), Analyses X PGT (resolution 135 eV). Images were acquired with a CDD Gatan 2 K × 2 K camera. Particle size was measured with UTHSCSA ImageTool software Version 3.0 Final. TGA measurements were recorded on a TGA7 Perkin-Elmer or Setaram 92.16.18 apparatus operating between 20 and 1500 °C. Curves were recorded between 20 and 1000 °C (20 °C min^{-1}) using an Al_2O_3 sample boat, and nitrogen as a vector (1 L h^{-1}).

Synthesis of the amino-PEG550

Synthesis of *O*-methanesulfonyl-*O′*-methylpolyethylene glycol 550 (2b). Commercial *O*-methylpolyethylene glycol 550 **2a** (27.9 g, 48 mmol, 1 eq.) was dried by heating at 80 °C overnight under vacuum. The material was then dissolved in dry dichloromethane (100 mL), and freshly distilled triethylamine (62.5 mmol, 8.7 mL, 1.3 eq.) was added. The mixture was cooled at 0 °C and methanesulfonylchloride (62.5 mmol, 4.9 mL, 1.3 eq.) was added dropwise under stirring over 15 min. After addition of all the reagents, the mixture was stirred at the same temperature for an additional 15 min., then at room temperature overnight. The resulting heterogeneous solution was filtered and the filtrate concentrated to dryness. The oil was dissolved in dichloromethane (200 mL) and washed twice with water (30 mL). The combined aqueous layers were extracted 3 times with dichloromethane (100 mL). The combined organic layers were then dried over $MgSO_4$, filtered and the solvent was evaporated to obtain 26.5 g of compound **1** (yield 98%). ^{1}H NMR ($CDCl_3$, 300.13 MHz): δ = 3.08 (3H, CH_3SO_3, *s*); 3.38 (3H, CH_3O, *s*); 3.48–3.58, (2H, CH_2OCH_3, *m*); 3.59–3.71 (43H, CH_2O, *m*); 3.72–3.82 (2H, CH_2O, *m*); 4.23–4.55 (2H, CH_2OSO_2, *m*). ^{13}C {^{1}H} NMR ($CDCl_3$, 75.47 MHz): δ = 37.66 (CH_3SO_3); 58.95 (CH_3O); 68.95 (CH_2O); 69.31 (CH_2OSO_2); 70.45, 70.50, 70.56 (CH_2O); 71.87 (CH_2OCH_3). MS (Maldi TOF,

dithranol, NaI): *m*/*z* range for [MNa^+] from 397.2 (5 CH_2CH_2O units) to 1019.6 (19 CH_2CH_2O units) separated by 44 Da (CH_2CH_2O); the most intense peak was at 661.4 (11 CH_2CH_2O units).

Synthesis of *O*-(2-ethylazido)-*O′*-methylpolyethylene glycol 550 (2c). **2b** (14 g, 21.90 mmol, 1 eq.) was dissolved in *N*,*N*-dimethylformamide (50 mL) and sodium azide (5.7 g, 87.7 mmol, 4 eq.) was added. The schlenk was flushed with argon and the mixture stirred in a pre-warmed oil bath at 80 °C. After 10 h the resulting mixture was diluted with water (20 mL) and stirred for a further 30 min. The mixture was extracted 6 times with dichloromethane (125 mL). The combined organic layers were then dried over $MgSO_4$, filtered and the solvent was evaporated. To perform the drying the oil was lyophilized to obtain 12.6 g of compound **2** (yield 98%). ^{1}H NMR ($CDCl_3$, 400.13 MHz): δ = 3.31–3.43 (5H, CH_3O and CH_2N_3, *m*); 3.49–3.58, (2H, CH_2OCH_3, *m*); 3.58–3.78 (47H, CH_2O, *m*). ^{13}C {^{1}H} NMR ($CDCl_3$, 75.47 MHz): δ = 50.67 (CH_2N_3); 59.02 (CH_3O); 70.02, 70.51, 70.56, 70.62, 70.66, 70.69 (CH_2O); 71.92 (CH_2OCH_3). MS (Maldi TOF, dithranol, NaI): *m*/*z* range for [MNa^+] from 344.2 (5 CH_2CH_2O units) to1004.6 (20 CH_2CH_2O units) separated by 44 Da (CH_2CH_2O); the most intense peak was at 608.4 (11 CH_2CH_2O units).

Synthesis of *O*-(2-ethylamino)-*O′*-methylpolyethylene glycol 550 (2d). Azidoethyl-polyethyleneglycol mono methyl ether **2c** (12.1 g, 20.66 mmol, 1 eq.) was dissolved in dry tetrahydrofurane (200 mL) and triphenylphosphine (8.13 g, 31 mmol, 1.5 eq.) was added. The homogeneous solution was stirred 4 days at room temperature, then hydrolysed with water (50 mL) and stirred for a further 5 h. The solution was evaporated at 50 °C under 60 mBar to obtain a mixture of oil and white solid (triphenylphosphine oxide). The mixture was solubilised in water (200 mL) and filtrated to partially eliminate the phosphine oxide. The aqueous layer was extracted 5 times with benzene (50 mL). The aqueous layer was evaporated at 50 °C under 60 mBar and lyophilized to perform the drying. The procedure gave 10.9 g of (**2d**) as a light yellow oil (yield 94%). ^{1}H NMR ($CDCl_3$, 300.13 MHz): δ = 1.76 (2H, NH_2, bs); 2.87 (2H, CH_2NH_2, *t*, $^3J_{H-H}$ = 5.1 Hz); 3.38 (3H, CH_3O, *s*); 3.52 (2H, $CH_2CH_2NH_2$, *t*, $^3J_{H-H}$ = 5.1 Hz); 3.54–3.62, (2H, CH_2OCH_3, *m*); 3.62–3.82 (44H, CH_2O, *m*).^{13}C {^{1}H} NMR ($CDCl_3$, 100.62 MHz): δ = 41.75 (CH_2NH_2); 59.02 (CH_3O); 70.28, 70.51, 70.57, 70.60 (CH_2O); 71.93 (CH_2OCH_3), 73.30 (CH_2CH_2 NH_2). MS (pos-ESI-TOF): *m*/*z* range for [MH^+] from 340.2 (6 CH_2CH_2O units) to 824.5 (17 CH_2CH_2O units) separated by 44 Da (CH_2CH_2O); the most intense peak was at 560.4 (11 CH_2CH_2O units).

Synthesis of the silica-dendrimer core–shell particle

Si-2. A suspension of **Si-1** (1.95 g) in absolute ethanol (90 mL) was added to 50 mL of a 2% weight solution of γ-aminopropyltriethoxysilane in distillated water. The suspension was heated at 85 °C during one day. After cooling, the new silica was filtered, washed with ethanol (4 × 50 mL), dichloromethane (4 × 50 mL) and diethyl ether (4 × 50 mL), in that order. The resulting material was dried under vacuum at 100 °C during 2 days to obtain 2.1 g of finely divided particle. ^{13}C CP-MAS NMR: δ = 9.73 (CH_2–Si); 26.88 (CH_2–CH_2–CH_2); 43.34 (CH_2–NH_2). ^{29}Si CP-MAS NMR: δ = −109.25 (Q_4 site); −100.22 (Q_3 site); −67.54 (T_3 site); −59.48 (T_2 site).

Si-3. To a solution of dendrimer **1-G$_1$** (215 mg, 75 μmol) in 140 mL of a mixture MeOH/THF (7 : 3, v/v) was added 300 mg of silica **Si-2**. The suspension was heated at 55 °C overnight. After cooling, the silica was separated by filtration on a sintered glass filter, washed with THF (4 × 50 mL) and dichloromethane (4 × 25 mL) and dried under vacuum at 100 °C to obtain 350 mg of **Si-3**. The filtrate was evaporated and the unreacted dendrimer was precipitated to afford 153 mg of a white powder. ^{31}P CP-MAS NMR: δ = 9.59 (P_0); 60.70 (P_1). ^{13}C CP-MAS NMR: δ = 10.80 (CH_2–Si); 23.39 (CH_2–CH_2–CH_2); 32.88 (CH_3–N); 43.34 (CH_2–NH_2); 50.7 (residual methanol); 62.63 (CH_2–N=); 121.67 (CH_{ar}); 132.98 (CH_{ar}); 139.90 (HC=N–NMe); 151.76 (CH_{ar}); 160.30 (HC=N); 189.90 (CHO) ^{29}Si CP-MAS NMR: δ = −109.81 (Q_4 site); −101.32 (Q_3 site); −66.42 (T_3 site); −59.04 (T_2 site).

Si-4. To a suspension of **Si-3** (205 mg) in methanol (2 mL) was added a solution of **2d** (35 mg; 62 μmol) in methanol (3 mL). After one day at room temperature the solvent was evaporated to dryness. ^{31}P CP-MAS NMR: δ = 9.10 (P_0); 61.25 (P_1). ^{13}C CP-MAS NMR: δ = 10.38 (CH_2–Si); 22.81 (CH_2–CH_2–CH_2); 32.80 (CH_3–N); 42.77 (CH_2–NH_2); 50.7 (residual methanol); 58.47 (CH_3–O); 60.96 (CH_2–N=); 70.56 (O–CH_2–CH_2–O); 121.72 (CH_{ar}); 130.07 (CH_{ar}); 133.09 (CH_{ar}); 139.31 (HC=N–NMe); 151.97 (CH_{ar}); 161.09 (HC=N). ^{29}Si CP-MAS NMR: δ = −110.08 (Q_4 site); −101.34 (Q_3 site); −65.94 (T_3 site); −56.67 (T_2 site).

Si-5. To 140 mg of silica **Si-3** was added 1.5 mL of dimethylphosphite used as solvent and reactant. After one day at room temperature 20 mL of dichloromethane was added to the mixture. The silica was separated by filtration on a sintered glass filter, washed twice with 25 mL of EtOH/H_2O (7 : 3, *v*/*v*), ethanol (4 × 25 mL) and dichloromethane (4 × 25 mL). The resulting silica was dried under vacuum at 65 °C during 2 days to obtain 150 mg of **Si-5**. ^{31}P CP-MAS NMR: δ = 8.99 (P_0); 25.78 (PO_3Me_2); 63.37 (P_1). ^{13}C CP-MAS NMR: δ = 10.50 (CH_2–Si); 22.19 (CH_2–CH_2–CH_2); 33.11 (CH_3–N); 42.73 (CH_2–NH_2); 52.91 ($POCH_3$); 58.80 (CH_3–O) 60.88 (CH–PO_3Me_2); 70.88 (O–CH_2–CH_2–O); 121.81 (CH_{ar}); 129.89 (CH_{ar}); 132.29 (CH_{ar}); 139.50 (HC=N–NMe); 151.19 (CH_{ar}). ^{29}Si CP-MAS NMR: δ = −109.81 (Q_4 site); −101.39 (Q_3 site); −66.42 (T_3 site).

Synthesis of Ag NPs on dendrimer-modified SiO_2 NPs

To a suspension of 50 mg of grafted silica (**Si-2**, **Si-3** or **Si-5**) in milli-Q water (2.5 mL) was added 2.5 mL of a solution of silver acetate in milli-Q water (1 g L^{-1}) corresponding to 15 μmol. The resulting mixture was left under stirring for one hour and then separated in two aliquots. One aliquot was left under stirring for two additional weeks (**Ag^{II}@Si-X** samples). The other aliquot was reacted with 600 μL of a solution of sodium borohydride in milli-Q water (2 g L^{-1}) corresponding to 16 μmol and left under stirring for 18 additional hours (**Ag^0@Si-X** samples). Electron microscopy samples were prepared by deposition of a small drop of crude suspensions onto carbon coated grids. After the appropriate time of reaction the different samples of silica were purified by 10 successive runs of centrifugation (2 min at 5000 rpm) and washing with milli-Q water (7 ml). Then the silica samples were freeze-dried.

Bacterial strains and culture conditions

The 4 tested strains belong to 4 potent pathogenic species obtained from the Institute Pasteur Collection (Paris, France): *Staphylococcus aureus* CIP 4.83, *Escherichia coli* CIP 103571, *Enterococcus hirae* CIP 58.55, *Pseudomonas aeruginosa* CIP 104116. The strains were stored at −80 °C in Eugon broth (AES, Rennes, France) with 20% (*v*/*v*) glycerol (Fluka, Butch, Switzerland) and reactivated at 37 °C under aerobic conditions on trypcase soy agar medium agar plates (Biomérieux, Craponne, France).

Antibacterial activities, MIC and MBC determination

The tested compounds were dissolved in sterile distilled water to obtain an initial concentration of 1000 ppm (silver equivalents) for the tested samples. Owing to compounds availability the initial concentrations were 500 ppm and 100 ppm respectively for **Ag^{II}@Si-3** and **Ag^{II}@Si-5**. Samples without silver were diluted to obtain the same concentration of SiO_2 as for the samples with silver. 100 μL of the resulting solutions were then diluted in the first wells of microtiter plates in 100 μL trypcase soy broth (Biomérieux, Craponne, France). Twofold serial dilutions were then performed from well 1 to well 10. Bacteria were grown overnight in trypcase soy broth at 37 °C until reaching stationary phase culture. Bacterial suspensions were then washed by centrifugation (3500 rpm, 5 min) and optical density adjusted in sterile distilled water to obtain 108 bacteria/mL and the microplate was then inoculated to obtain a final concentration of 106 bacteria/ml (Denley multipoint inoculator). After 24 h of incubation at 37 °C, the MICs were defined as the lowest concentrations with no visible growth. Rows 11 and 12 were used for growth negative control and positive control, respectively. The Minimal Bactericidal Concentrations (MBC) were defined as the concentrations that cause bacterial death (>99% of the population) and were checked by lack of macroscopic sign of cellular growth after subcultivating the MICs cultures on trypcase soy agar plates for 24 h at 37 °C. All experiments were carried out in duplicate at each concentration.

Acknowledgements

We acknowledge financial support from the CNRS. This work has been partially supported by the French National Agency (ANR; COPPERTREE, project N° ANR-11-BS07-018).

Notes and references

1 A. M. Caminade, C. O. Turrin, R. Laurent, A. Ouali and B. Delavaux-Nicot, *Dendrimers. Towards catalytic, material and biomedical uses.*, Wiley & Sons Ltd, Chichester, 2011.
2 G. Schmid, in *Nanoparticles: From theory to applications (second edition)*, ed. G. Schmid, Wiley VCH, Weinheim, 2010.
3 R. W. J. Scott, O. M. Wilson and R. M. Crooks, *J. Phys. Chem. B*, 2005, **109**, 692–704.
4 M. Q. Zhao, L. Sun and R. M. Crooks, *J. Am. Chem. Soc.*, 1998, **120**, 4877–4878.
5 A. El Kadib, N. Katir, M. Bousmina and J. P. Majoral, *New J. Chem.*, 2012, **36**, 241–255.
6 C. O. Turrin, V. Maraval, A. M. Caminade, J. P. Majoral, A. Mehdi and C. Reye, *Chem. Mater.*, 2000, **12**, 3848–3856.
7 N. Tsubokawa, H. Ichioka, T. Satoh, S. Hayashi and K. Fujiki, *React. Funct. Polym.*, 1998, **37**, 75–82.
8 K. Sakai, T. C. Teng, A. Katada, T. Harada, K. Yoshida, K. Yamanaka, Y. Asami, M. Sakata, C. Hirayama and M. Kunitake, *Chem. Mater.*, 2003, **15**, 4091–4097.
9 J. P. K. Reynhardt and H. Alper, *J. Org. Chem.*, 2003, **68**, 8353–8360.
10 S. Antebi, P. Arya, L. E. Manzer and H. Alper, *J. Org. Chem.*, 2002, **67**, 6623–6631.
11 G. Larsen and S. Noriega, *Appl. Catal., A*, 2004, **278**, 73–81.
12 D. R. Radu, C. Y. Lai, K. Jeftinija, E. W. Rowe, S. Jeftinija and V. S. Y. Lin, *J. Am. Chem. Soc.*, 2004, **126**, 13216–13217.
13 A. V. Biradar, A. A. Biradar and T. Asefa, *Langmuir*, 2011, **27**, 14408–14418.
14 S. P. Ramnani, S. Sabharwal, J. V. Kumar, K. H. P. Reddy, K. S. R. Rao and P. S. S. Prasad, *Catal. Commun.*, 2008, **9**, 756–761.
15 Q. D. Viet, P. B. Sarawade, A. Hilonga, J.-K. Kim, Y. G. Chai, S. H. Kim, J.-Y. Ryu and H. T. Kim, *Appl. Surf. Sci.*, 2011, **257**, 6963–6970.
16 J.-S. Hwang, K.-Y. Chen, S.-J. Hong, S.-W. Chen, W.-S. Syu, C.-W. Kuo, W.-Y. Syu, T. Y. Lin, H.-P. Chiang, S. Chattopadhyay, K.-H. Chen and L.-C. Chen, *Nanotechnology*, 2010, **21**, 025502.
17 M. A. Villegas, M. A. Garcia, S. E. Paje and J. Llopis, *Mater. Res. Bull.*, 2005, **40**, 1210–1222.
18 Y. W. Zhang, H. S. Peng, W. Huang, Y. F. Zhou and D. Y. Yan, *J. Colloid Interface Sci.*, 2008, **325**, 371–376.
19 N. Launay, A. M. Caminade, R. Lahana and J. P. Majoral, *Angew. Chem., Int. Ed. Engl.*, 1994, **33**, 1589–1592.
20 E. Trevisiol, V. Le Berre-Anton, J. Leclaire, G. Pratviel, A. M. Caminade, J. P. Majoral, J. M. Francois and B. Meunier, *New J. Chem.*, 2003, **27**, 1713–1719.
21 B. Miksa, S. Slomkowski, M. M. Chehimi, M. Delamar, J. P. Majoral and A. M. Caminade, *Colloid Polym. Sci.*, 1999, **277**, 58–65.
22 M. Avella, F. Bondioli, V. Cannillo, E. D. Pace, M. E. Errico, A. M. Ferrari, B. Focher and M. Malinconico, *Compos. Sci. Technol.*, 2006, 886–894.
23 N. Mejías, R. Pleixats, A. Shafir, M. Medio-Simón and G. Asensio, *Eur. J. Org. Chem.*, 2010, 5090–5099.
24 T. Akiyama, M. Sanada and K. Fuchibe, *Synlett*, 2003, 1463–1464.
25 A. A. Sobanov, A. V. Zolotukhin, V. I. Galkin, O. A. Mostovaya, R. A. Cherkasov and A. N. Pudovik, *Russ. J. Gen. Chem.*, 2003, **73**, 871–876.
26 R. A. Cherkasov and V. I. Galkin, *Russ. Chem. Rev.*, 1998, **67**, 857–882.
27 L. Griffe, M. Poupot, P. Marchand, A. Maraval, C. O. Turrin, O. Rolland, P. Métivier, G. Bacquet, J. J. Fournié, A. M. Caminade, R. Poupot and J. P. Majoral, *Angew. Chem., Int. Ed.*, 2007, **46**, 2523–2526.
28 A. Hameau, C.-O. Turrin and A.-M. Caminade, unpublished results.
29 G. S. Caravajal, D. E. Leyden, G. R. Quinting and G. E. Maciel, *Anal. Chem.*, 1988, **60**, 1776–1786.

30 C. H. Chiang, N. I. Liu and J. L. Koenig, *J. Colloid Interface Sci.*, 1982, **86**, 26–34.
31 G. Schmid, E. Emmrich, J. P. Majoral and A. M. Caminade, *Small*, 2005, **1**, 73–75.
32 C. O. Turrin, V. Maraval, J. Leclaire, E. Dantras, C. Lacabanne, A. M. Caminade and J. P. Majoral, *Tetrahedron*, 2003, **59**, 3965–3973.
33 H. Xu, F. Yan, E. E. Monson and R. Kopelman, *J. Biomed. Mater. Res.*, 2003, **66A**, 870–879.
34 H. Ibrahim, A. Furiga, E. Najahi, C. P. Henocq, J. P. Nallet, C. Roques, A. Aubouy, M. Sauvain, P. Constant, M. Daffe and F. Nepveu, *J. Antibiot.*, 2012, **65**, 499–504.
35 J. Azéma, B. Guidetti, A. Korolyov, R. Kiss, C. Roques, P. Constant, M. Daffé and M. Malet-Martino, *Eur. J. Med. Chem.*, 2011, **46**, 6025–6038.
36 K. Kawahara, K. Tsuruda, M. Morishita and M. Uchida, *Dent. Mater.*, 2000, **16**, 452–455.
37 Q. L. Feng, J. Wu, G. Q. Chen, F. Z. Cui, T. N. Kim and J. O. Kim, *J. Biomed. Mater. Res.*, 2000, **52**, 662–668.
38 V. Dal Lago, L. F. de Oliveira, K. D. Goncalves, J. Kobarg and M. B. Cardoso, *J. Mater. Chem.*, 2011, **21**, 12267–12273.
39 J. R. Morones, J. L. Elechiguerra, A. Camacho, K. Holt, J. B. Kouri, J. T. Ramirez and M. J. Yacaman, *Nanotechnology*, 2005, **16**, 2346–2353.